Elsevier Editorial System(tm) for Journal of the European Ceramic Society

Manuscript Draft

Manuscript Number:

Title: New ceramic materials from MSWI bottom ash obtained by an innovative microwave-assisted sintering process

Article Type: Full Length Article

Keywords: bricks, MSW, sintering process, microwave

Corresponding Author: Prof. Alexander Karamanov, PhD

Corresponding Author's Institution: Institute of Physical chemistry

First Author: Rosa Taurino

Order of Authors: Rosa Taurino; Alexander Karamanov, PhD; Roberto Rosa; Emilia karamanova; Luisa Barbieri; Stela Atanasova-Vladimirova; Georgi Avdeev; Cristina Leonelli

Abstract: Preliminary results on the production of new ceramic bricks by microwave-assisted sintering process employing MSWI bottom ashes are reported.
Microwave heating technique was compared with a conventional thermal treatment with the aims to: (1) study the influence of heat treatment method on crystallization behavior and microstructure of obtained samples; (2) define the crystallization evolution in microwave field; (3) gain an insight into the physical properties of the new samples.
Higher crystallinity and new crystal phases were observed in the samples prepared by microwave heating, where precipitation of new sodium rich crystal phases was observed, together with quartz and anorthite, formed in conventionally prepared samples.
The possibility to obtain novel bricks with huge waste amount, in a very short thermal cycle and at relatively low temperatures was demonstrated with significant reductions in the energy demand for their production.
Finally, the samples obtained by microwave-assisted sintering are characterized by improved mechanical properties.

Suggested Reviewers: Dachamir Hotza Prof.
dhotza@gmail.com

Rosiza Nikolova Prof.
rosica.pn@clmc.bas.bg

Maximina Romero Prof.
mromero@ietcc.csic.es

*Cover Letter

Bulgarian Academy of Sciences
Institute of Physical Chemistry

SOFIA 1113, BULGARIA
Acad. G. Bonchev Str., bl. 11

phone: (+359 2) 872-00-21
fax: (+359 2) 971-26-88

March 28, 2016
Sofia

Dear Editor

We would like to submit our paper entitled “New ceramic materials from MSWI bottom ash obtained by an innovative microwave-assisted sintering process” by R. Taurino, R. Rosa, E. Karamanova, L. Barbieri, S. Atanasova-Vladimirova, G. Avdeev, C. Leonelli and myself for publication in the “Journal of the European Ceramic Society”.

Sincerely yours,

Alexander Karamanov

AUTHOR'S PHONE NUMBER
+359.2.979 2552

AUTHOR'S FAX NUMBER
+359.2.9712688

AUTHOR'S EMAIL
karama@ipc.bas.bg

AUTHOR'S POSTAL ADDRESS
Prof. Dr. Alex Karamanov
Department of Amorphous Materials
Institute of Physical Chemistry
BULGARIAN ACADEMY OF SCIENCES
"Ac. G. Bontchev" str., bl 11
1113 SOFIA
BULGARIA

***Summary of Novel Conclusions**

Novel MSWA bricks, obtained with low cost microwave heat-treatment, were compared with conventionally treated samples. The results elucidate higher crystallinity, formation of new crystal phases and improved exploitation properties.

New ceramic materials from MSWI bottom ash obtained by an innovative microwave-assisted sintering process

R. Taurino[1*], A. Karamanov[2*], R. Rosa[1], E. Karamanova[2], L. Barbieri[1],

S. Atanasova-Vladimirova[2], G. Avdeev[2], C. Leonelli[1]

[1]Department of Engineering "Enzo Ferrari", University of Modena and Reggio Emilia, Via Vivarelli 10, 41125, Modena, Italy.

[2]Institute of Physical Chemistry, Bulgarian Academy of Sciences, Acad. G. Bonchev Str., bl.11, 1113 Sofia, Bulgaria.

corresponding authors e-mail:
rosa.taurino@unimore.it, rosa.taurino@unipr.it and
karama@ipc.bas.bg

Abstract

Preliminary results on the production of new ceramic bricks by an innovative microwave-assisted sintering process employing MSWI bottom ashes are reported.

Microwave heating technique was compared with a conventional thermal treatment with the aims to: (1) study the influence of heat treatment method on the crystallization behavior and on the microstructure of obtained samples; (2) define the crystallization evolution in microwave field; (3) gain an insight into the physical properties of the new samples.

Higher crystallinity and new crystal phases were observed in the samples prepared by microwave heating, where precipitation of new sodium rich crystal phases was observed, together with quartz and anorthite, formed in the conventionally prepared samples.

The possibility to obtain novel bricks with huge waste amount, in a very short thermal cycle and at relatively low temperatures was demonstrated with significant reductions in the energy demand for their production.

Finally, the samples obtained by microwave-assisted sintering are characterized by improved mechanical properties.

Keywords: bricks, MSW, sintering process, microwave.

Introduction

Recently, the predominant industrial waste treatments have been solidification and thermal processes, encouraging alternatives to land disposal and to manufacturing processes requiring extensive energy consumption. Concurrently, more efficient resource recovery alternatives should be studied. One of the main waste that can be considered as new raw material for ceramic and building sector is the bottom ash produced during the incineration of Municipal Solid Waste (MSW).

Among the methods for the valorization of bottom ash, the preparation of glass-ceramics, ceramics and glasses seem to be promising for converting MSWI (municipal solid waste incineration) bottom ash into novel materials that possess attractive mechanical and chemical properties[1-4]

Particularly, several studies employing MSWI ash were carried out in order to evaluate the chemical durability of the vitrified products, the crystallization behavior of the parent glasses, the structure and properties of bulk glass-ceramics as well as the possibility to obtain different sintered ceramics and glass-ceramics by conventional heating technologies. Thermal treatment, such as sintering, has been proposed to convert MSWI bottom ash into ceramic-type materials [1-4]. In

addition to the many advantages of these eco-friendly new materials, a novel and innovative technology could be used to save energy and to improve the sintering processes. In this latter perspective, the use of microwaves represents an alternative sintering strategy to manufacture ceramic materials, with several potential benefits.

In particular, this study investigated the feasibility to combine clay and MSWI bottom ash in the production of bricks with properties comparable to those of conventionally made bricks. Publications, mostly in the form of patents, exist on this topic, mainly discussing methods of microwave drying of bricks [5-9], nevertheless, no studies reported the microwave assisted sintering behaviour of bricks based on high amount of waste.

Since the MSWI bottom ash is a poor receptor of microwave energy, a "hybrid microwave sintering" process was used in this study to achieve the temperature necessary for preparing ceramic materials. In particular, a specific experimental set-up with a peculiar geometry was designed for preparing samples starting from an "end of waste" derived from the industrial processing of MSWI bottom ash.

Furthermore, the aim this paper was to study the influence of heat treatment schedule on the crystallization behavior and microstructure of the microwave-prepared ceramic materials. In addition, investigation was performed to gain an insight into the physical properties of the ceramics prepared by microwaves in comparison to those obtained by conventional heating [1,10], exploiting a conventional process

2. Experimental

2.1 Materials

The raw material used in this study is an artificial silica-based aggregate, rich in Ca, Al and Fe, with controlled grain size, derived from a MSWI bottom ash treatment plant in the North of Italy. The applied treatment mainly consists of three steps: (i) 3 months ageing of the as received bottom ash coming from several incinerators mainly in the North-Centre of Italy leading to uptake of CO_2 from the air, drying of excess water and partial oxidation; (ii) mill grinding to obtain two fractions with particle size of 0–2 mm and 2–8 mm; (iii) separation of metallic iron and aluminium by means of magnetic and eddy current systems.

The separated metals, appropriate for recycling, are ~ 8 wt% (7% Fe and 1% Al) of the total amount while the bottom ash recovered as secondary raw material (SRM) is ~80 wt%; the remaining ~10 wt% is water evaporated during the ageing treatment and unburnt organic part of the waste.

In this study the fraction between 2–8 mm, which is the predominant part of the aggregate obtained, was used. The bottom ash appeared as a gray grainy powder. Its main chemical composition is given in Table 1. After 2 hours of heat-treatment at 600°C to definitively burn the organic residues, the bottom ash with the other raw materials were milled in a ball mill until a homogeneous particle size was obtained.

Other raw materials, used for the preparation of the ceramics batches, were industrial kaolin (K), Na_2CO_3 and corundum powder (Al_2O_3) (below 54 microns). The chemical composition of MSWI bottom ash (BA) and kaolin were examined by X-ray fluorescence spectroscopy (ARL ADVANT'XP X-ray fluorescence spectrometer) and the results are shown in Table 1.

2.2 Preparation of ceramic green bodies

Three different ceramic formulations were studied (Table 2). The ceramic batch (labelled C-b) was obtained by mixing 55 wt% of heat-treated BA and 45 wt% of kaolin (K) with 7 wt% of water. In the other two ceramics (labelled C-b-Al and C-b-Na) 5% of BA was substituted by fine (below 54 microns) corundum powder and Na_2CO_3, respectively.

Samples of 50 x 5 x 4 mm^3 were prepared by cold isostatically pressing the above mentioned powders at 40 MPa with a dwell time of 30 seconds. These samples have been dried overnight before firing. The average green density was 1.8 ± 0.3 g/cm^3 (calculated on the basis of the weight of the ignited sample). These samples were used for dilatometric studies of the sintering process.

2.3 Sintering of ceramic bodies

Conventional heating

In the conventional process, samples were heated in an optical dilatometry (Expert System Solutions, Misura HSML ODLT 1400) at 30°C/min up to 1000°C and held to this temperature for 5 min. The holding temperature and time were selected, using preliminary DTA and dilatometric results [10].

Microwave hybrid heating experimental set-up

The microwave sintering experiments were carried out in a multimode microwave cavity operating at the frequency of 2.45 GHz (CEM MAS 7000-CEM, USA), which was equipped with a circular mode stirrer placed on the upper wall, in order to improve the heating homogeneity. The magnetron generator had a nominal maximum power of 950 W. Microwave power was set to its maximum in all the experiments. Surface temperature measurements were performed by means of a K-type thermocouple. The arrangement of the sample inside the microwave cavity is schematically

depicted in Fig. 1. As clearly visible, both a microwave-absorbing material layer (SiC) and a microwave-transparent material layer (Al_2O_3) were used, the latter being positioned on the top surface in order to avoid the reflection loss of the incident wave on the front surface between the reactor and air. The MW absorbing layer is able to absorb the incident wave transmitted through the MW transparent layer and consequently to generate heat. In terms of optimizing the arrangement of the samples during microwave assisted sintering experiment, the dielectric properties of the selected materials and the thickness of each layer are the most important parameters to control.

In this framework, several preliminary experiments allowed the selection of 7 mm and 13 mm as the optimal thicknesses for the transparent and the absorbing layers respectively for sample with size of 13 mm and 3.5 mm as diameter and height, respectively.

Sintering experiments were conducted at three different maximum temperatures (800-900-1000°C). In all cases an isothermal holding of 5 min was made.

2.4 Characterization of samples

The thermal behavior of the parent batches was estimated by differential thermal analysis, using Netzsch STA 409 apparatus. The applied heating rate was 20°C min^{-1} up to 1250°C. To study the sintering process, bar samples (50mm x 5 mm x 4 mm) were fired in an optical dilatometer (Expert System Solutions, Misura HSML ODLT 1400).

The chemical analysis was performed with XRF spectrometry (ARL ADVANT'XP X-ray fluorescence spectrometer). Argon was used as the inert gas.

Physical characteristics of linear shrinkage (LS), water absorption (WA) and measurement of weight loss of ignition (WLOI%) were performed according to ISO 10545-3[12]. The apparent density, ρ_a, of the sintered samples was estimated by precise measurement of dimensions and weight of the sample, while the skeleton, ρ_s, and absolute, ρ_{as}, densities were determined by Ar pycnometer (AccuPyc 1330, Micromeritic). The results were used to evaluate total P_T, closed P_C, and open P_O porosity according to the following equations 1-3:

$$P_T = 100 \times (\rho_{as} - \rho_a)/ \rho_{as} \quad (1)$$

$$P_C = 100 \times (\rho_{as} - \rho_S)/ \rho_{as} \quad (2)$$

$$P_O = 100 \times (\rho_s - \rho_a)/ \rho_{as} \quad (3)$$

The experimental errors in the evaluations ρ_a, ρ_s, and ρ_{as}, were $\pm$ 0.03, $\pm$ 0.01 and $\pm$ 0.01 g/cm^3 leading to mistakes of at about 2% for the total and open porosity and at about 1 % for closed porosity, respectively. The experimental errors for LS and WA were ± 0.5 % and 1 %, respectively.

XRD analysis was conducted to identify the crystalline phases obtained in conventional and microwave treatment. The X-ray diffraction (XRD) pattern was recorded using a conventional Bragg-Brentano powder diffractometer (Empyrcam, Panalytical) with a Ni-filtered Cu-Kα radiation using bracket holder. The scanning was done in the range of 2θ angle from 5° to 70° with a step size of 0.02°. The obtained peaks are compared with ICCD in order to identify the crystalline phases.

Microstructural and chemical analyses were carried out using Scanning Electron Microscopy, SEM (JEOL, JSM 6390) and energy dispersive x-ray spectroscopy (INCA, Oxford Instruments). The accelerating voltage was 20 kV, and the current I ~65 μA. The analyses were made using fractured samples, coated with Au.

Fired products were characterized for mechanical properties like compressive strengths by an electro-mechanical Instron 3300 (Instron, MA, USA).

Results and discussion

Thermal behavior

Fig. 2 shows the DTA plots of C-b, C-b-Al and C-b-Na. The endo-effects related to kaolinite deoxydrilation are identical for all compositions (endothermic events around 540-560°C). The crystallization exo-peaks due to reactions between the formed meta-kaolin and the phases from BA and the first melting endo-effect for C-b-Al and C-b are detected at 985-980°C and 1160–1200°C, respectively, for both samples. It can be concluded that the corundum powder does not influence the crystalline phase formation and their subsequent melting, so that it can be considered as an inert addition.

On the contrary, the addition of Na_2O significantly decreases both temperatures of phase formation and melting (approximately of 120 and 90^{o}C, respectively), which highlights its obvious fluxing effect.

The sintering behavior of studied samples in the range 20–1000°C was evaluated by optical dilatometer and the obtained results for the variations of linear shrinkages, as well as the used temperature regime are plotted in Fig. 3.

The densification curves show a shrinkage of about 0.3-0.5% at about 600°C due to the kaolinite dehydration. Then, in C-b and C-b-Al samples the densification starts at about 900 °C and practically ends after 3-4 min holding at 1000°C (i.e. after the formation of new phases according to the DTA results). The reached shrinkage in C-b-Al is lower due to a reduced sintering rate (a consequence of the addition of inert corundum powder).

In C-b-Na samples, the densification starts at about 800 °C and finishes at about 950°C with a shrinkage of about 2.5 %, which is similar to the C-b-Al one.

Physical and mechanical properties

Table 3 shows the results of all density measurements of microwave and conventionally processed samples, while Table 4 summarized the corresponding porosity values and the results for the linear shrinkage (LS%), water absorption (WA%) and weight loss of ignition (WLOI).

The differences in the absolute densities between C-b and C-b_{MW}, as well as between C-b-Al and C-b-Al_{MW} might be attributed to a different crystallinity (i.e. higher is the crystallinity higher is ρ_{as}), while the variations in C-b-Na indicate variation in the phase compositions due to the applied method of heat-treatment.

It can be noted that C-b-Na sample, treated with microwave heat-treatment at 1000°C, completely melted inside the SiC "covering", then the results are not reported in the table. It should be noted that the same composition, treated by conventional heat-treatment, start to deform at about 1200°C (i.e. at higher with 200^{o}C temperature)[10].

The porosity evaluations in MW samples elucidate that the increasing of temperature decreases the total porosity of 3-5 %, as well as that at higher temperatures some closed porosity is formed. At the same time, in the C-b and C-b-Al samples, conventionally treated at 1000^{o}C, the porosity remains exclusively open, notwithstanding that the total porosity is similar to that of the corresponding MW samples. Only in sample C-b-Na_{1000} some closed porosity was evidenced.

The quality of a building brick can be measured by evaluation of its firing shrinkage and water absorption (WA). A good quality brick can exhibit a linear LS lower than 8%, while according to the criteria listed in CNS 382 [12,13], a first class brick must have a WA value lower than 15%, a second-class brick must have 15-19% water absorption and the third-class brick calls for WA lower than 23%.

Our results highlighted that all laboratory samples, sintered at 900 and 1000^{o}C, categorically met both criteria for a first class brick: indeed the linear shrinkage and the water absorption are below 4 % and 14%, respectively. In addition, because of the formation of closed porosity, WA values of C-b_{1000MW} and C-b-Al_{1000MW} are lower than 10%, which is a particularly worth to note result.

The weight loss for a normal clay brick usually is 15% [12,13]. In the studied samples, due to the usage of huge amount of pre-treated MSWI, WLOI results are significantly lower, which also can be considered as an encouraging result.

The most important engineering quality index for the building bricks is their compressive strength. According to ASTM C-67[14], the minimum required compressive strength of a paving brick subjected to light traffic is 17.2-20.7 MPa14[15].

The compressive strength of samples obtained by conventional heat-treatment at 1000^{o}C, as well as of the samples obtained in microwave furnace at 900^{o}C, were measured and compared. The results are summarized in Fig. 4 and elucidate the all the obtained values (especially ones for C-b and C-b-Al) significantly surpass the limit for the compressive strength.

Moreover, notwithstanding of the lower firing temperatures, the microwave heated samples at 900^{o}C attained a high compressive strength of 60-65 MPa. This behavior is a consequence of the difference in crystallinity and microstructure and will be highlighted in the next sections.

XRD analysis

X-ray diffraction analysis (XRD) was carried out to identify the crystalline phases in both conventional and microwave processed samples.

For the conventional samples, sintered at 1000°C (Fig. 5), the major phases were quartz (SiO_2) [JCPDF file 01-078-1252] and anorthite ($CaAl_2Si_2O_8$) [JCPDF file 00-002-0523], with traces of albite ($Na_2O.Al_2O_3.6SiO_2$) [JCPDF file 01-083-1610] in C-b-Na and corundum [JCPDF file 01-071-1124] in C-b-Al.

The results for the samples obtained by microwave treatments, at 800, 900 and 1000 °C, are summarised in Fig. 6. This data clearly highlight an enhanced crystallization and appearance of new phases.

The microwave-sintered samples C-b_{MW} (Fig. 6a) showed that at 800^{o}C the main phases are quartz and gehlenite deriving from the initial BA waste component, while at 900^{o}C the amount of these phases decreases due to formation of anorthite and a new calcium aluminium oxide phase ($CaAl_2O_4$) [JCPDF file 00-034-0440]. This process of phase transformations continues also at 1000^{o}C, resulting in the higher final crystallinity in comparison with sample C-b_{1000} (see Fig. 5).

The phase formation of C-b-Al_{MW} samples shows similar behavior as the one in C-b_{MW} with an expected occurrence of inert corundum appearance.

In our previous studies with conventionally treated C-b and C-b-Al samples[10] it was demonstrated that at 900^{o}C, in accordance with the DTA results shown in Fig. 2, an evident formation of anorthite is not yet observed. This difference clearly highlights one of the widely recognized drawbacks of microwaves-assisted processes, i.e. the difficulty of exact temperature measurement, with a firing temperature under-estimated of about 100^{o}C. At the same time a faster heating rate of the samples was estimated, indicating that microwave hybrid heating is an energy efficient method to fire these

novel ceramic formulations. The final advantage of the microwave assisted was an undoubted increase in the bending strength values of all samples.

X-ray diffraction measurement of sample C-b-Na_{900MW}, shows (Fig. 6c) that together with the formation of sodian anorthite solid solutions [JCPDF file 01-084-0750], high amount of nepheline ($(Na,K)AlSiO_4$) [JCPDF file 01-083-2372] was also formed. This interesting behaviour might be related to a local formation of a "transitory sodium rich liquid phase" with low viscosity and subsequent crystallization.

In fact, in a heterogeneous system, such as the used bottom ash, a mixture of crystalline and amorphous components [1,16,17] with different melting temperatures is present. Generally, in similar batches the alkaline and alkaline earth oxides are the most reactive components, resulting in the formation of an intergranular thin liquid phase involving mass transport phenomena and locally wetting of the solid grains. Thus, the addition of "free Na_2O" as a fluxing agent accelerates the "local" melting at lower temperatures and improves the low temperature sintering. In this study a further acceleration of this reaction mechanism could be due to the microwave irradiation itself, which is known to act via a volumetric heat transfer of energy from the electromagnetic wave to the solid sample [7,8]. The localized formation of the liquid phases enhances the mechanism of heat transfer and accelerate the ions diffusion at the interface with the solid grains. This peculiarity will be studied in details in a future research.

SEM analysis

The structure of final C-b_{1000}, C-b-Na_{1000} and C-b-Al_{1000} samples were studied in detail by SEM-EDS and the results were already published and discussed[10]. These observations highlighted that the surfaces and the fractures of specimens heat-treated at 1000^{o}C in a traditional electric furnace are similar and are characterized by an irregular structures and open porosity. Some closed porosity was observed only in C-b-Na_{1000}, which can be explained with its lower crystallinity. The main crystalline phases are residual α-quartz and newly formed plagioclase (anorthite or anorthite-albite solid solution). Residual gehlenite, some pyroxene, as well as little glass or ceramic debris and fine corundum particles (in C-b-Al_{1000}) were also observed.

Typical images at low magnification of surface (C-b_{1000}) and fracture (C-b-Al_{1000}), showing a ceramic body with a suitable degree of sintering for bricks production[18,19] and typical open porosity, are presented in Figs. 7-a and 7-b , respectively. In Fig. 7-c the formation of closed porosity in sample C-b-Na_{1000} is elucidated.

Fig. 8 demonstrates typical images of the main crystal phases in the samples (together with the corresponding EDS spectra). In Figs. 8-a and 8-b non-reacted α-quartz and gehlenite are shown, respectively, while Fig. 8-c reports a glass piece from the parent BA. The presence of these residual phases might be explained with their relatively large sizes (more then 10-20 microns), which hinders their dissolution and/or transformation. At the same time, Fig. 8-d elucidates a typical anorthite crystal. The anorthite s.s. crystals formed after only 5 min at 1000^{o}C were not yet well shaped, with their hexagonal habit that was not clearly visible and the crystals size was in the range 3-6 microns.

In a previous study performed on similar compositions[1] heat-treated at 1200-1260^{o} C for 1 h, it was demonstrated that, with the increasing of temperature, gehlenite totally disappeared and the amount of quartz significantly decreased leading to an increasing of the anorthite phase percentage. At high temperature the single anorthite crystals got a very regular hexagonal shape but no significant increase in their crystal size was observed.

The structures of samples obtained by microwave treatment at different temperatures were also studied by SEM-EDS. It was clarified that at 800^{o}C, in accordance with the density and XRD data, the processes of densification and the phase formation remain in their initial stages. This is demonstrated in Figs. 9-a and 9-b, which show a "loose" bulk structure of sample C-b$_{800MW}$ and a small (10-15 microns) non-dissolved quartz particle, respectively.

The crystallographic and pycnometric results demonstrated that after microwave treatment at 900^{o}C the samples C-b-Al$_{900MW}$ and C-b-$_{900MW}$ showed porosity, phase composition and mechanical properties, similar to the ones obtained at 1000^{o}C in traditional furnace. The SEM observations confirmed these data highlighting also similar structure and morphology. In Figs. 10-a and 10-b are presented the top surface of C-b-Al$_{900MW}$ and the fracture surface of C-b$_{900MW}$, while Figs. 10-c elucidates the newly formed anorthite crystals. It is interesting to note that these anorthite crystals have a significantly smaller size with respect to those formed in the sample obtained by traditional heat-treatment. A lower size of the formed crystal phase in ceramics, obtained by microwave sintering was observed also in other compositions where a fast and volumetric heating was reached and a uniform nucleation rate was recorded ex-post [20-21]

The increasing of temperature in samples C-b-Al$_{1000MW}$ and C-b$_{900MW}$ did not lead to a notable improvement of the densification. However, the amount of tiny anorthite crystals increased, which

might be mainly related to a better dissolution of the quartz phase thanks to localized formation of liquid phase as discussed above. Fig. 10-d highlights a large quartz grain, where the dissolution process is in an advanced stage.

The formation of nepheline, imbedded in Si and Al reach zone of sample C-b-Na_{900MW}, is shown in Fig. 11–a, while melted glassy drops from C-b-Na_{1000MW}, inside the SiC capsule, is presented in Fig. 11-b.

From scientific point of view, notwithstanding of the lower mechanical properties, the results recorded for the C-b-Na_{MW} samples are the most intriguing. It was already noted that sample C-b-Na_{1000MW} totally melted inside the SiC "capsule", while the corresponding sample, C-b-Na_{1000}, melts at about 1200^{o}C. At the same time, the XRD analysis of sample C-b-Na_{900MW} (see Fig.6-c) demonstrated the new formation of a high amount of nepheline, (Na,K)$AlSiO_4$, which was totally absent in the samples obtained in conventional heat-treatment.

The presence of nepheline phase cannot be explained by the chemical composition of the new ceramic formulation and by its position in QAPF (Quartz, Alkali feldspar, Plagioclase, Feldspathoid) mineralogical phase diagram[22,23.] This observation rather indicates that nepheline formation is a result of "local" reactions caused by MW heat-treatment. Most probably, the crystallization of nepheline is a result of reaction between the metakaolin ($Al_2Si_2O_7$) and free Na_2O.

The melting temperature of nepheline is relatively high (>1500^{o}C), but this phase has very low eutectic temperatures with albite and other phases, which partially might explain the melting of the sample C-b-Na_{1000MW}. This phenomenon will be studied in near future.

Conclusions

The possibility to obtain new ceramics, based on high amount (up to 55 wt%) of pre-treated bottom ash from municipal solid waste incinerators, using microwave heat-treatment was shown. Samples with parameters (firing shrinkage, water absorption and compressive strength), corresponding to the standards for traditional clay bricks were obtained in extremely short heat-treatment of 5 min a temperature of 900°C. The volumetric heating, characteristic of microwave assisted processing, led to uniform formation of new anorthitic crystals and, when Na carbonate was added, also nepheline was found. The experimental set-up used for microwave hybrid heating contributed to a shift in temperature measurements of about 100°C lower than real temperature, nevertheless peculiar features were recorded with XRD, SEM and EDS observations.

The efficient heat transfer phenomenon due to microwave irradiation coupled with the use of MSWI bottom ash contributed to the manufacture of a particularly environment-friendly ceramic material characterized by energy and natural materials savings.

Acknowledgments

The authors are grateful for the financial support deriving from the program of mobility, scientific and cultural collaboration of the University of Modena and Reggio Emilia with the Institute of Chemical Physics of the Bulgarian Academy of Sciences (Sofia, Bulgaria) – 2012-2013.

References

[1] Schabbach LM, Andreola F, Barbieri L, Lancellotti I, Karamanova E, Ranguelov B, Karamanov A. Post-treated incinerator bottom ash as alternative raw material for ceramic manufacturing. *J Eur Ceram Soc* 2012,**32**:2843-52.

[2] Rambaldi E, Esposito L, Andreola F, Barbieri L, Lancellotti I, Vassura I. The recycling of MSWI bottom ash in silicate based ceramic. Ceram Int. 2010;**36**:2469–76.

[3] Schabbach L, Andreola F, Karamanova E, Lancellotti I, Karamanov A, Barbieri L. Integrated approach to establish the sinter-crystallisation ability of glasses from secondary raw material. *J Non-Crystalline Solids* 2011;**357**:10–7.

[4] Barbieri L, Corradi A, Lancellotti I, Manfredini T. Use of municipal incinerator bottom ash as sintering promoter in industrial ceramics. *Waste Manage* 2002;**22**:859-63

[5] Gyllis I, Xenos T. Processing of ceramic materials with radio-frequencies of the microwave and UHF zones both modulated or non-modulated, WO1991008177 A1, Public. date 13 giu 1991.

[6].Edwin E Childs Jr. Microwave method for tempering tar-bonded refractory bricks US3673288 A date 27 giu 1972

[7] Leonelli C, Veronesi P. Microwave Processing of Ceramic and Ceramic Matrix Composites. Book Chapter in *Ceramics and Composites Processing Methods*[7] Bansal NP, Boccaccini AR. editors, .John Wiley and Sons, Inc., Hoboken, NJ, 2012, pp. 485, ISBN: 978-047055344-2.

[8] Morteza O, Omid M. Microwave versus conventional sintering: A review of fundamentals, advantages and applications. *J Alloys and Comp*. 2010;**494**:175-89

[9] Shirai T, Yasuoka M, Hotta Y, Kinemuchi Y, Watari K. Drying behavior of a slip cast body using a microwave heating. *J Am Ceram Soc* 2008;**91**:2367-70

[10] Karamanov E, Taurino R, Andreola F, Atanasova-Vladimirova S, Barbieri L, Lancellotti I, Karamanov A. Compositions for novel ceramic bricks based on pretreated MSWA. Conference: Proceedings of the XV Balkan Mineral Processing Congress, Sozopol, Bulgaria, June 12–16, 2013, At Sozopol, Bulgaria, Volume: VOLUME II

[11] ISO 10545-3:1995 Ceramic tiles Part 3: Determination of water absorption, apparent porosity, apparent relative density and bulk density.

[12] Long KL.Feasibility Study of Using Brick made from Municipal Solid Waste Incinerator Fly Ash Slag. *J Hazard Mat*. 2006;**137**:1810-6.

[13] Lissy MPN,Sreeja MS. Utilization of sludge I Manufacturing Energy Efficient Bricks. *IOSR JMCE*. 2014;**11**:70-73

[14] ASTM C-67, 1992. Standard Test Method of Sampling and Testing Brick and Structural Clay Tile.

[15] Loryuenyong V, Panyachai T, Kaewsimork K, Siritai C. Effects of recycled glass substitution on the physical and mechanical properties of clay bricks. *Waste Manag*. 2009;29:2717–21.

[16] Lam CHK, Ip AWM, Barford JP, McKay G. Use of Incineration MSW Ash: A Review. *Sustainability* 2010;**2**:1943-68

[17] Li M, Kiang J, Hu S, Sun LS, Su S, Li PS, Sun XX. Characterization of solid residues from municipal solid waste incinerator. *Fuel* 2004;83:1397-405.

[18] Adeola JO. A review of masonry block/brick types used for building in Nigeria. MEng thesis, Univ of Benin. 1977.

[19] Karaman S, Ersahin S, Gunal H. Firing temperature and firing time influence on mechanical and physical properties of clay bricks. *J Sci Res* 2006;**65**:153-9.

[20] Boccaccini AR, Veronesi P, Leonelli C. Microwave processing of glass matrix composites containing controlled isolated porosity. *J Eur Ceram Soc* 2001;**21**:1073-1080.

[21] Yu T, Wei Z, Dongdong C. Crystallization evolution, microstructure and properties of sewage sludge-based glass-ceramics prepared by microwave heating. *J Hazard. Mat*. 2011;**196**:370-70

[22] Le Maitre, R.W.. Igneous Rocks: A Classification and Glossary of Terms: Recommendations of International. Union of Geological Sciences Subcommission on the Systematics of Igneous Rocks. *Cambridge University Press*, 2002, pp 236, ISBN 052166215X

[23] https://en.wikipedia.org/wiki/QAPF_diagram.

Table 1. Chemical composition (wt%) of two raw materials used (K = kaolin; BA = MSWI bottom ash).

OXIDE	**K**	**BA**
SiO_2	52.5	46.8
TiO_2	0.5	0.7
Al_2O_3	33.3	9.8
Fe_2O_3	0.6	4.3
CaO	0.2	18.6
MgO	0.4	2.9
K_2O	0.9	1.0
Na_2O	0.1	4.5
B_2O_3	0.0	0.6
MnO	0.0	0.3
ZnO	0.0	0.3
PbO	0.0	0.3
SO_3	0.0	1.0
P_2O_3	0.0	1.2
CuO	0.0	0.5

Table 2. Chemical composition (wt%) of the studied ceramics

Oxide	**C-b**	**C-b-Al**	**C-b-Na**
SiO_2	54.2	51.5	52.7
TiO_2	0.7	0.7	0.7
Al_2O_3	22.2	26.9	22.1
Fe_2O_3	3.1	2.7	2.8
CaO	11.6	10.5	10.7
MgO	2.0	1.8	1.8
K_2O	1.0	1.0	1.0
Na_2O	2.8	2.6	5.9
B_2O_3	0.4	0.3	0.3
MnO	0.2	0.2	0.2
ZnO	0.2	0.2	0.2
PbO	0.2	0.2	0.2
SO_3	0.6	0.5	0.5
P_2O_3	0.8	0.7	0.7
CuO	0.3	0.3	0.3

Table 3. Apparent (ρ_a), skeleton (ρ_s) and absolute (ρ_{as}) densities of microwave and conventionally-processed samples.

Sample	Processing route	Temperature (°C)	ρ_a (g/cm^3)	ρ_s (g/cm^3)	ρ_{as} (g/cm^3)
C-b$_{1000}$	Conventional	1000	1.86	2.67	2.69
C-b$_{1000MW}$	Microwave	1000	1.92	2.61	2.73
C-b$_{900MW}$	Microwave	900	1.89	2.67	2.73
C-b$_{800MW}$	Microwave	800	1.80	2.72	2.73
C-b-Al$_{1000}$	Conventional	1000	1.95	2.77	2.78
C-b-Al$_{1000MW}$	Microwave	1000	1.92	2.82	2.84
C-b-Al$_{900MW}$	Microwave	900	2.00	2.72	2.73
C-b-Al$_{800MW}$	Microwave	800	1.79	2.78	2.81
C-b-Na$_{1000}$	Conventional	1000	1.92	2.62	2.74
C-b-Na$_{1000MW}$	Microwave	1000	-	-	-
C-b-Na$_{900MW}$	Microwave	900	1.82	2.66	2.69
C-b-Na$_{800MW}$	Microwave	800	1.72	2.70	2.76

Table 4. Total porosity (P_T), open porosity (Po), closed porosity (Pc), linear shrinkage (LS%), water absorption (WA%) and weight loss of ignition (WLOI) of microwave and conventionally-processed samples.

Sample	Temperature (°C)	P_T (%)	Po (%)	Pc (%)	WA (%)	LS (%)	WLOI (%)
C-b$_{1000}$	1000	31	30	1	14	4	7.3
C-b$_{1000MW}$	1000	30	26	4	6	2.5	7.4
C-b$_{900MW}$	900	31	29	2	8	2.5	7.2
C-b$_{800MW}$	800	34	34	0	13	0.5	6.3
C-b-Al$_{1000}$	1000	30	29	1	13	3.5	6.9
C-b-Al$_{1000MW}$	1000	32	30	2	10	3	8.3
C-b-Al$_{900MW}$	900	27	26	0	9	2	7.8
C-b-Al$_{800MW}$	800	36	35	1	13	0.5	7.1
C-b-Na$_{1000}$	1000	30	26	4	12	3.5	10.6
C-b-Na$_{900MW}$	900	32	30	2	8	2.5	11.8
C-b-Na$_{800MW}$	800	36	34	2	12	2.0	10.4

Figures captions

Figure 1. A scheme of the geometry adopted for the hybrid heating experiments within the microwave furnace.

Figure 2. Non-isothermal DTA results of C-b (dot line), C-b-Al (solid line) and C-b-Na (dash line) compositions.

Figure 3. Dilatometer results for compositions C-b, C-b-Al and C-b-Na at heat-treatment of 30^{o}C/min heating rate, 5 minutes holding at 1000°C and free cooling.

Figure 4. Compressive strength (σ_c) of the samples conventionally-processed at 1000°C and microwave processed at 900°C.

Figure 5. XRD spectra of C-b_{1000}, C-b-Na_{1000} and C-b-Al_{1000} samples after conventional heating. Q: α-quartz [JCPDF file 01-078-1252], A: anorthite [JCPDF file 00-002-0523]; Co: corundum [JCPDF file 01-071-1124]; Al: albite [JCPDF file 01-083-1610].

Figure 6. XRD spectra of a) C-b, b) C-b-Al and c) C-b-Na samples treated by microwave . Q: α-quartz [JCPDF file 01-082-0511], A: anorthite, sodian [JCPDF file 00-020-0528], Ca: calcium aluminum oxide [JCPDF file 00-034-0440], N: nepheline [JCPDF file 00-019-1176], G:gehlenite [JCPDF file 01-087-0968].

Figure 7. SEM images of: a) C-b_{1000} sample surface,b) C-b_{Al1000} sample fracture and c) closed pore in C-b-Na_{1000} sample.

Figure 8 SEM images and spectra of: a) quartz particle (Q) and Corundum (C) in C-b-Al_{1000} sample, b) gehlenite (G) in C-b-Al_{1000} sample, c) glassy (g) debris in C-b-Na_{1000} and anorthite crystal (A) in C-$b_{1000.}$

Figure 9. a) SEM image of C-b_{800MW} sample fracture and b) SEM image and EDS spectrum of Quartz particle (Q) in C-b_{800MW} sample.

Figure 10. SEM images of a) C-b-Al900MW sample surface, b) C-b900MW sample fracture, c) a typical zona of tiny plagioclase crystals in C-b900MW sample and d) quartz grain (Q) in stage of dissolution in C-b1000MW sample.

Figure .11. a) SEM image and EDS spectrum of large (15-25 microns) nepheline structure in C-b-Na_{900MW} sample and b) SEM image of "melted" part of sample C-b-$Na_{1000MW.}$

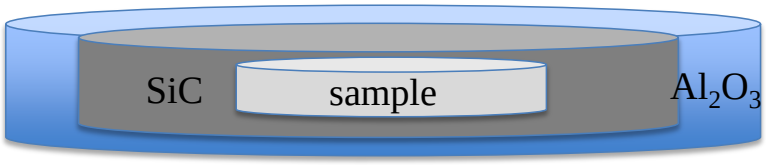

Fig. 1

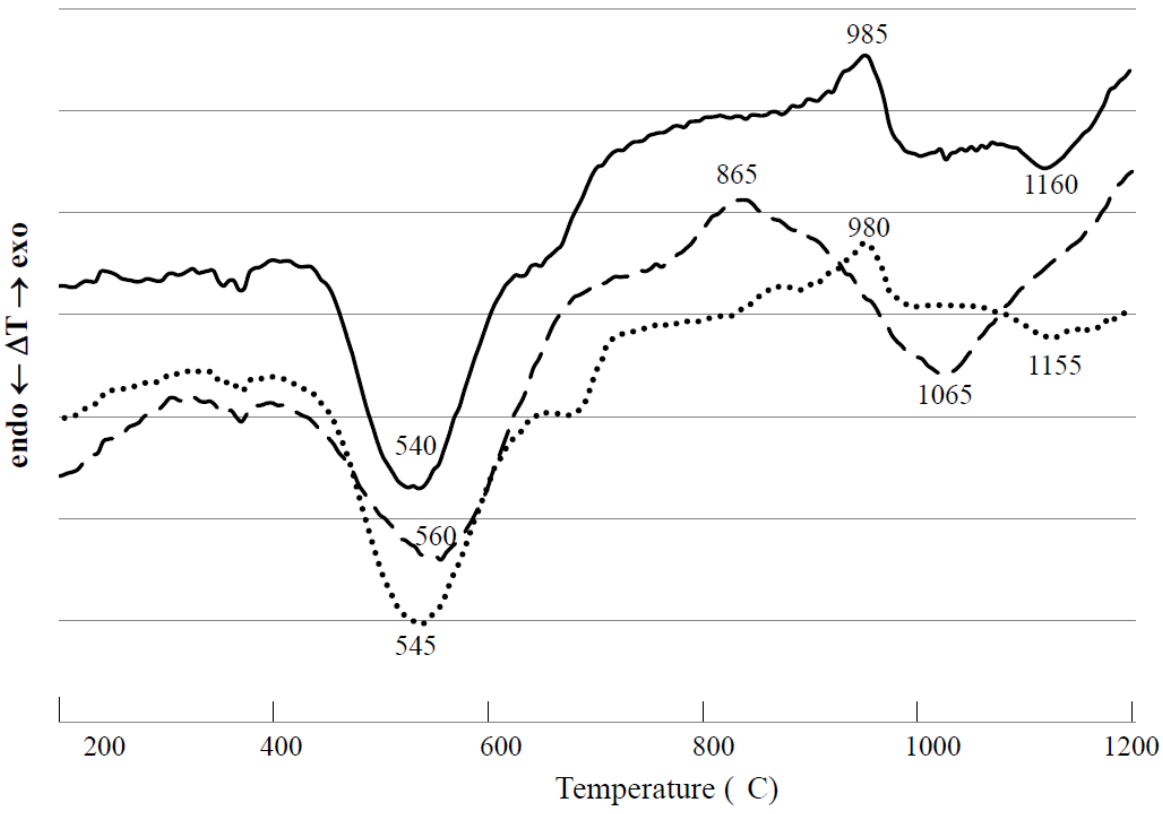
985
865
980
1160
1155
1065
540
560
545
endo ← ΔT → exo
200
400
600
800
1000
1200
Temperature (C)

Fig. 2.

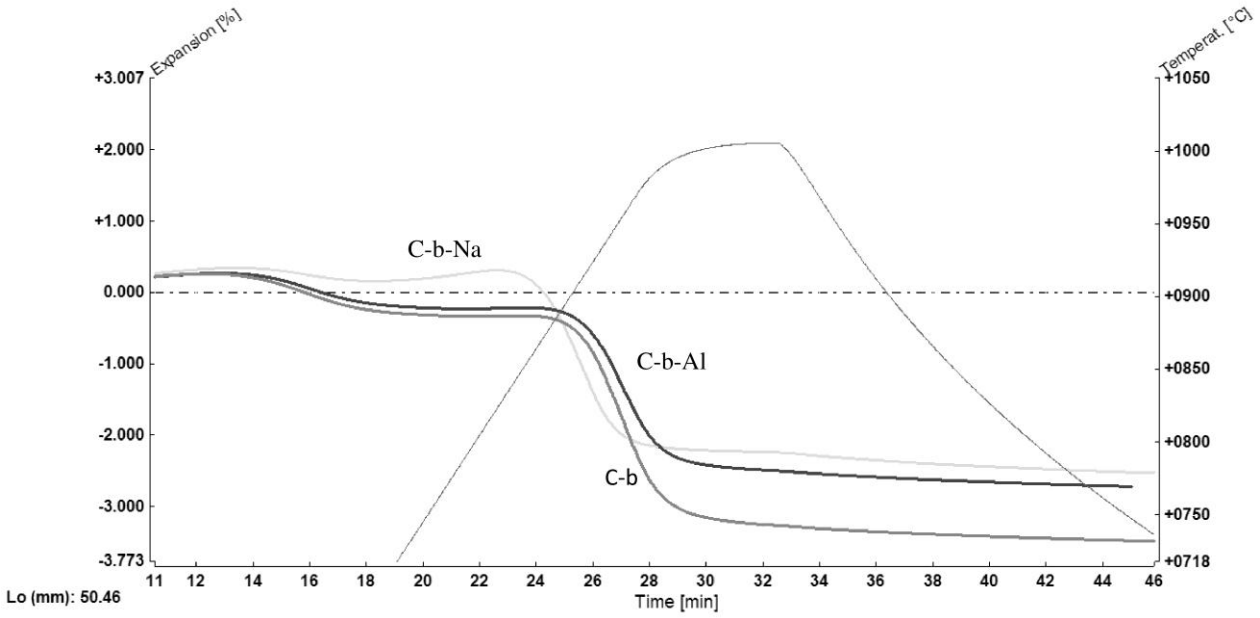
Expansion [%]
Temperat. [°C]
+3.007
+2.000
+1.000
0.000
-1.000
-2.000
-3.000
-3.773
+1050
+1000
+0950
+0900
+0850
+0800
+0750
+0718
C-b-Na
C-b-Al
C-b
11 12 14 16 18 20 22 24 26 28 30 32 34 36 38 40 42 44 46
Time [min]
Lo (mm): 50.46

Fig. 3.

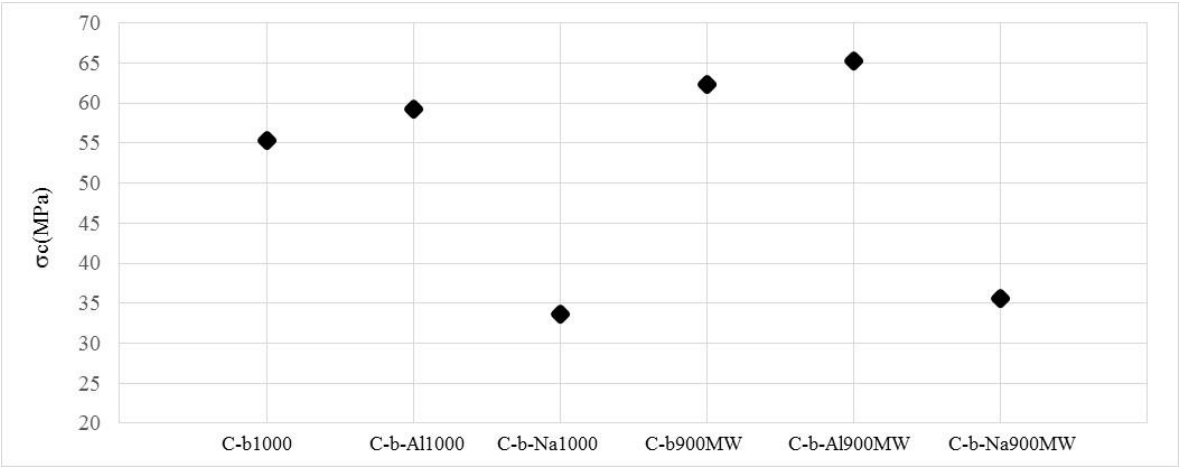
70
65
60
55
50
45
40
35
30
25
20
σc(MPa)
C-b1000
C-b-Al1000
C-b-Na1000
C-b900MW
C-b-Al900MW
C-b-Na900MW

Fig. 4.

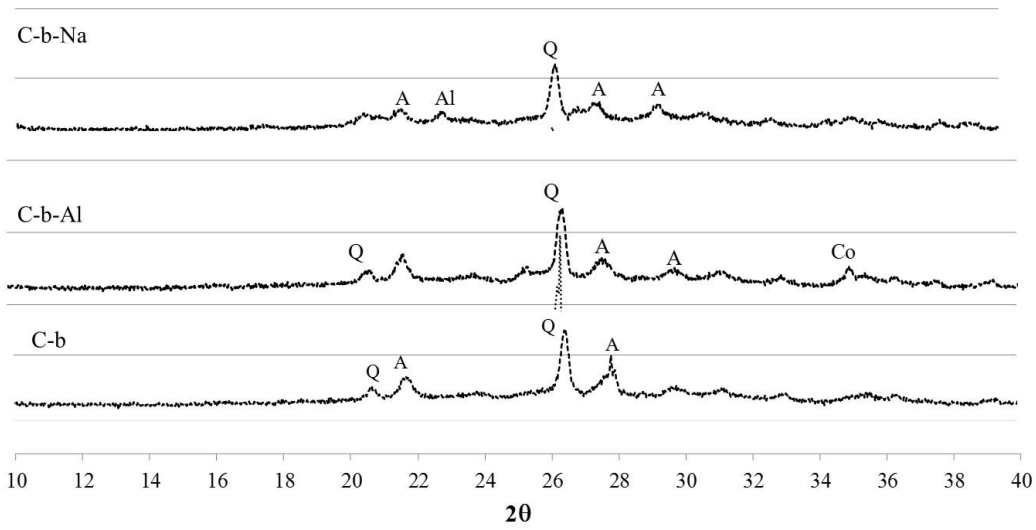
C-b-Na
Q
A
Al
A
A
C-b-Al
Q
Q
A
A
Co
C-b
Q
Q
A
A
10
12
14
16
18
20
22
24
26
28
30
32
34
36
38
40
2θ

Fig. 5

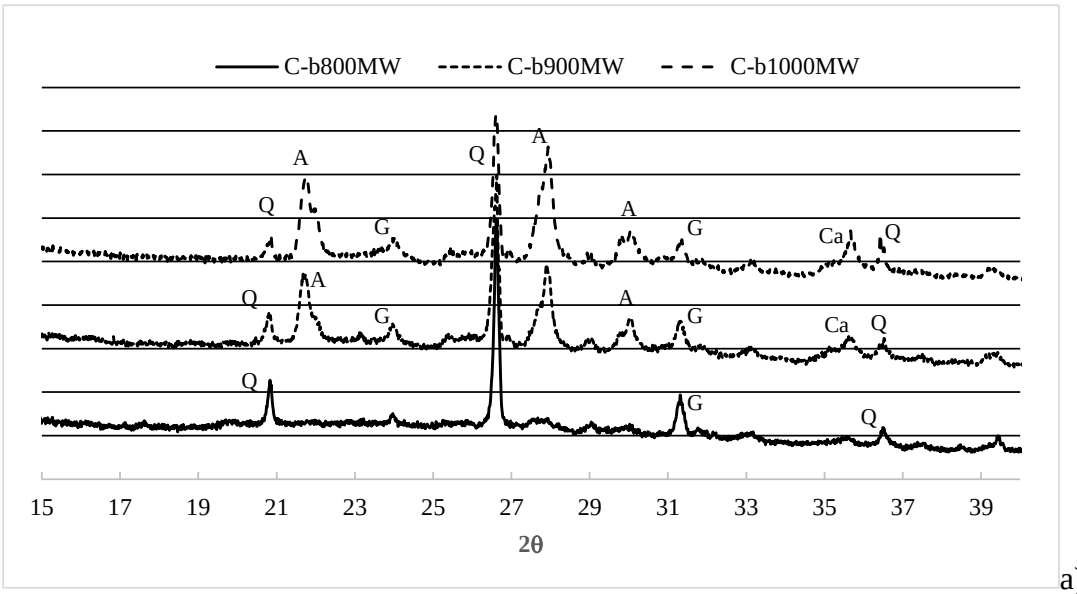
C-b800MW
C-b900MW
C-b1000MW
Q
A
G
Ca
15 17 19 21 23 25 27 29 31 33 35 37 39
2θ

a)

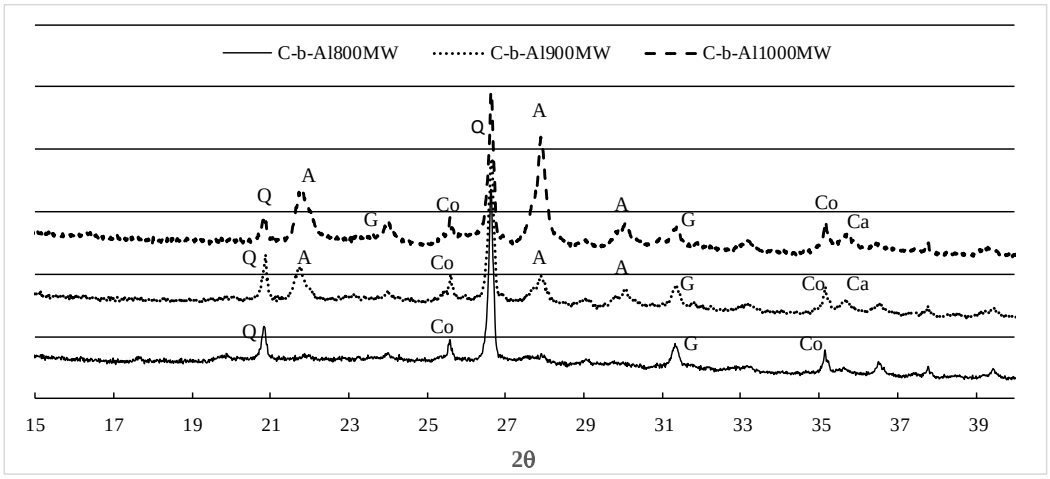
C-b-Al800MW
C-b-Al900MW
C-b-Al1000MW
Q
A
G
Co
Ca
15 17 19 21 23 25 27 29 31 33 35 37 39
2θ

b)

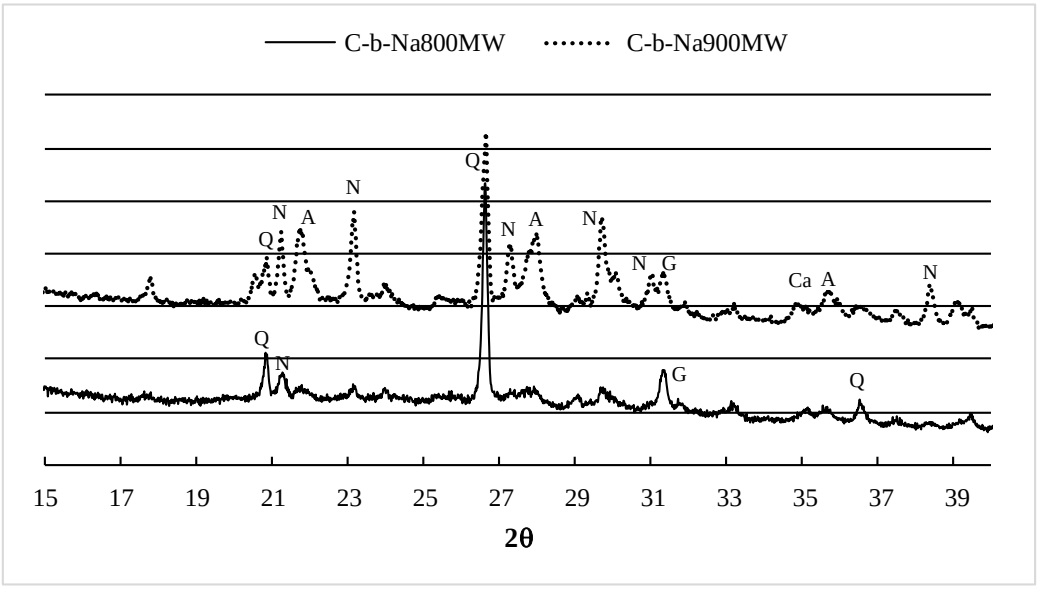
C-b-Na800MW
C-b-Na900MW
Q
N
A
G
Ca
15 17 19 21 23 25 27 29 31 33 35 37 39
2θ

c)

Fig. 6.

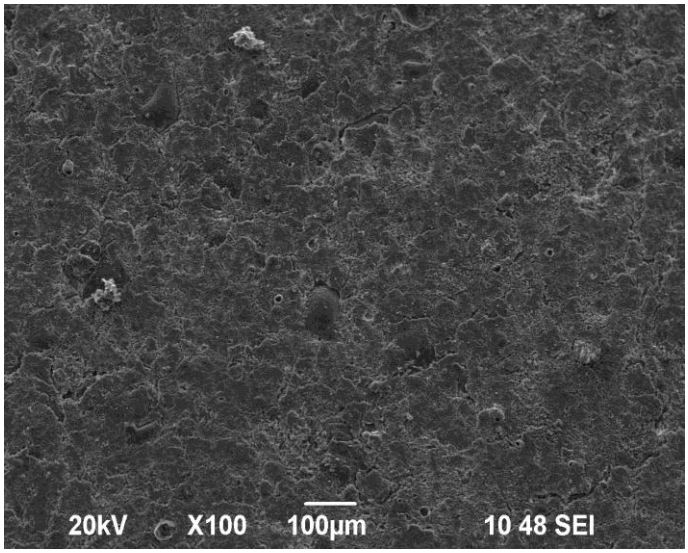
20kV X100 100µm 10 48 SEI
a)

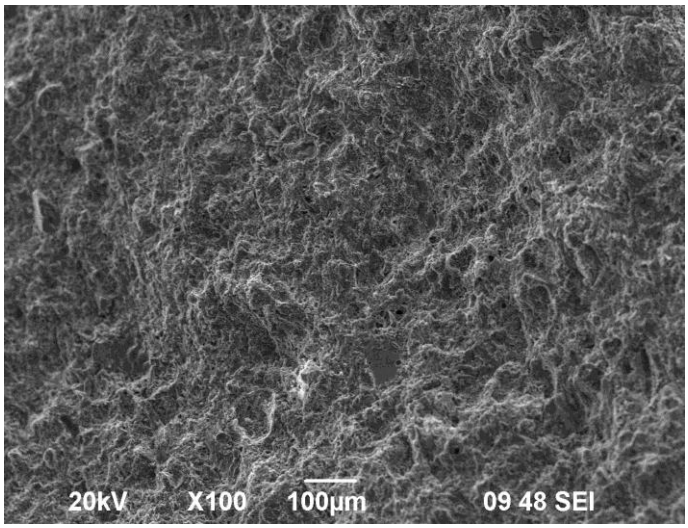
20kV X100 100µm 09 48 SEI
b)

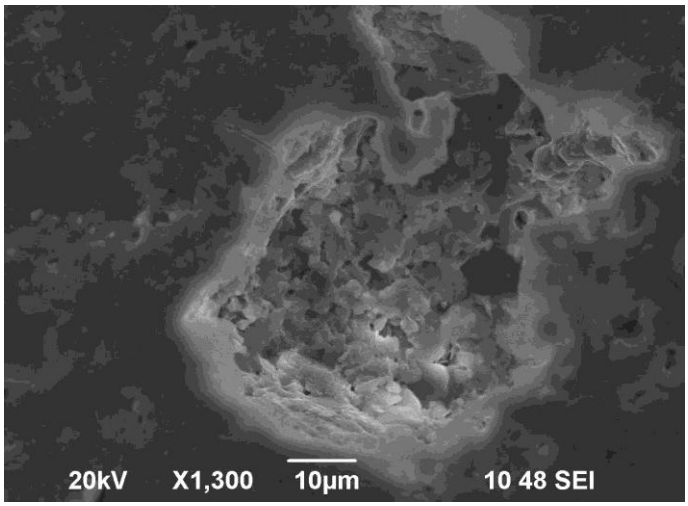
20kV X1,300 10µm 10 48 SEI
c)

Fig. 7

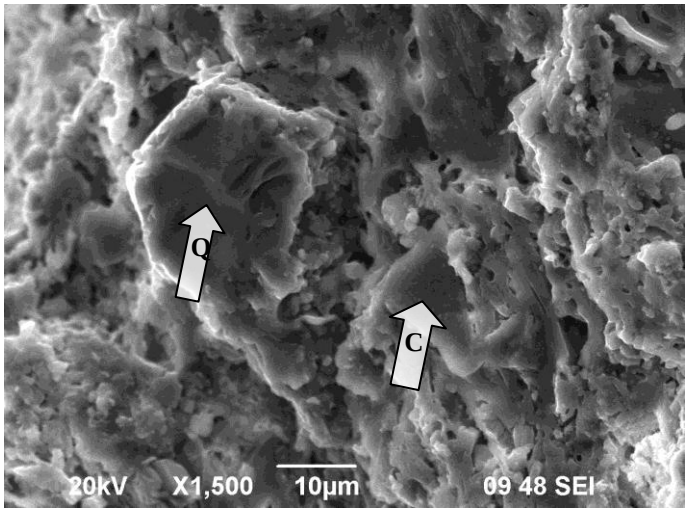

a)

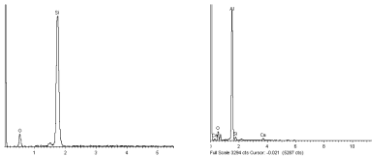

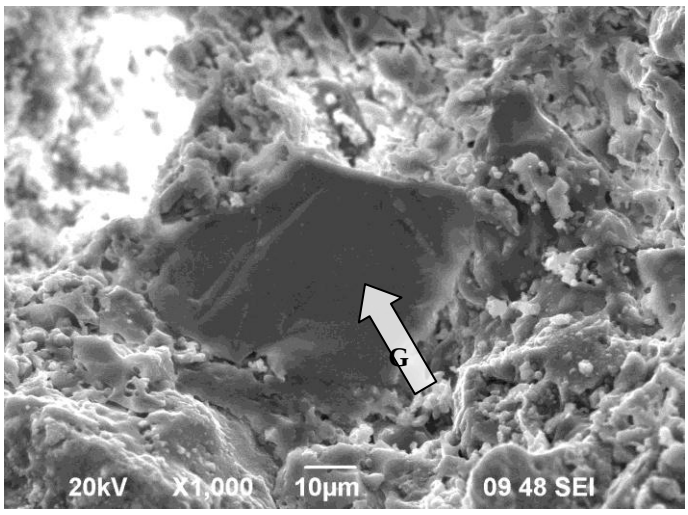

b)

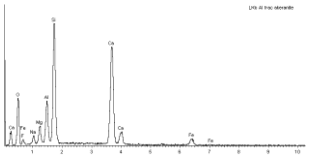

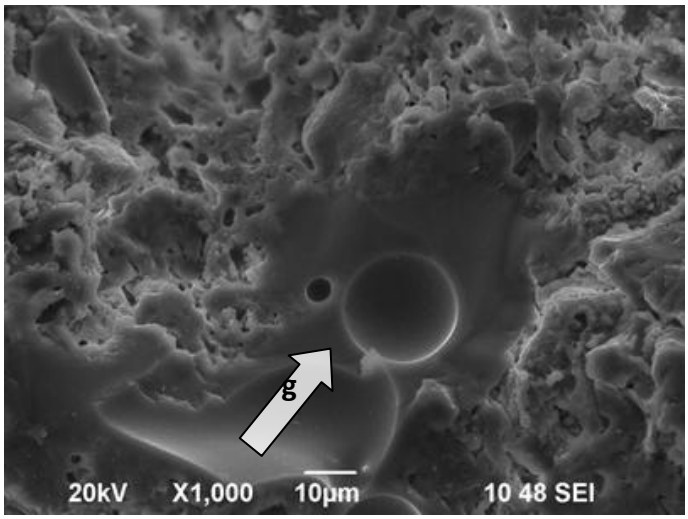

c)

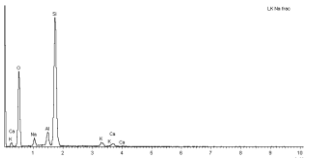

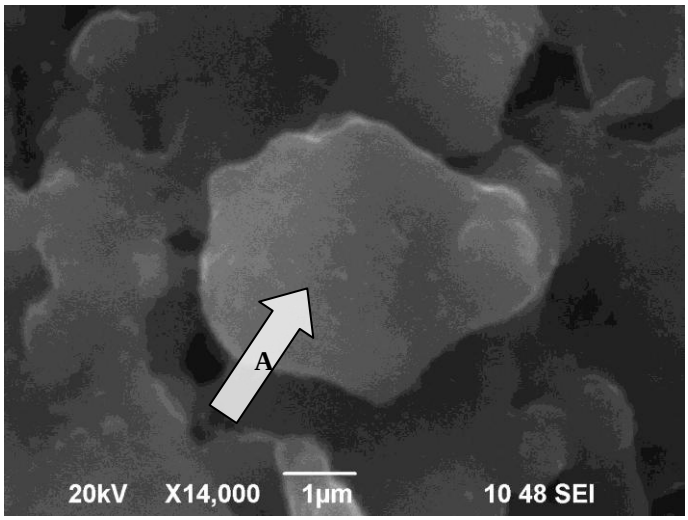

d)

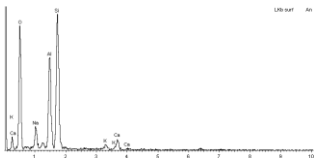

Fig. 8

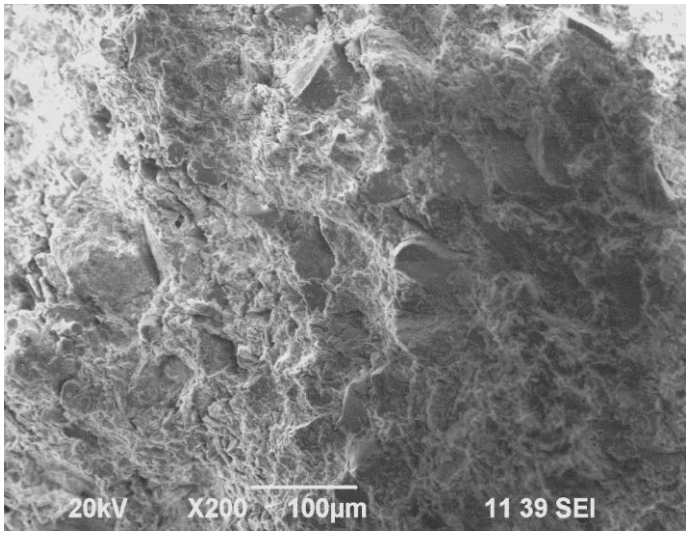

a)

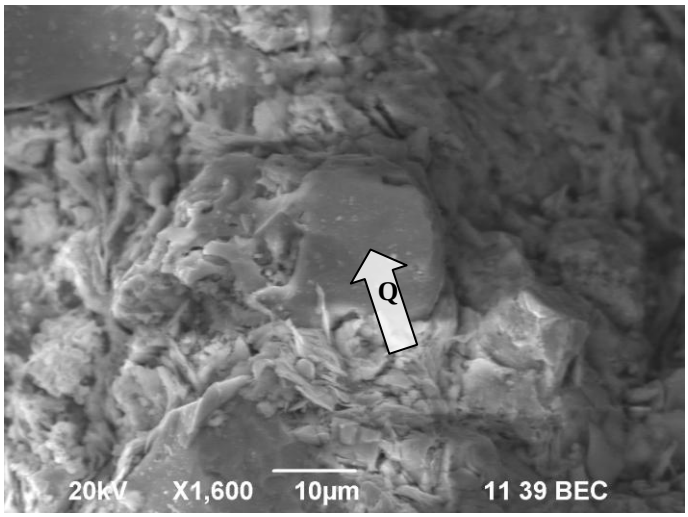

b)

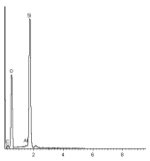

Fig. 9

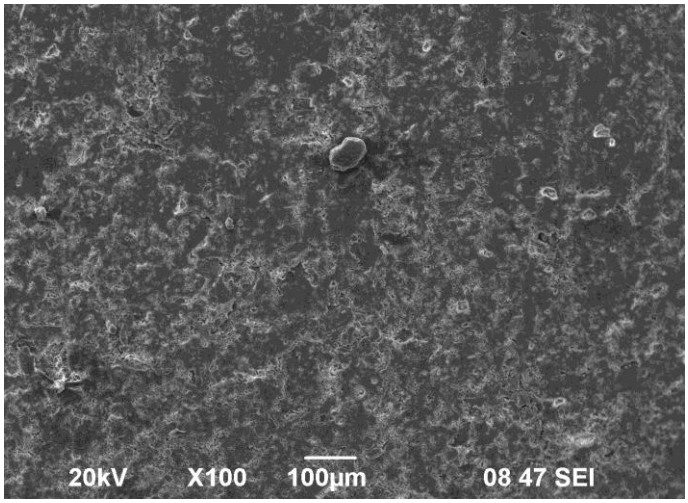

a)

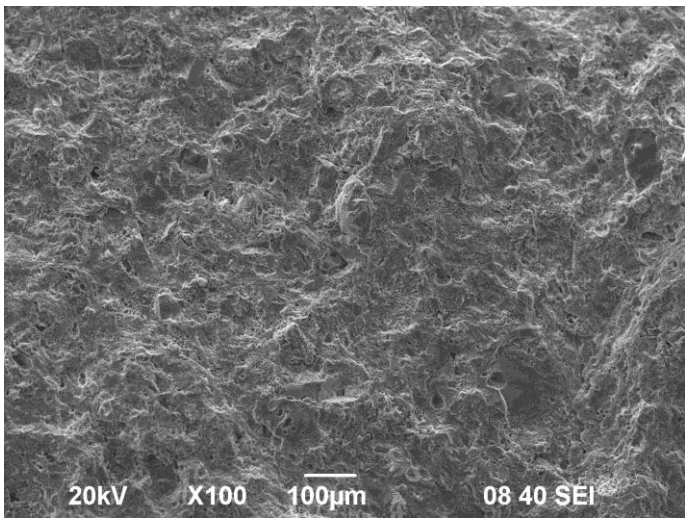

b)

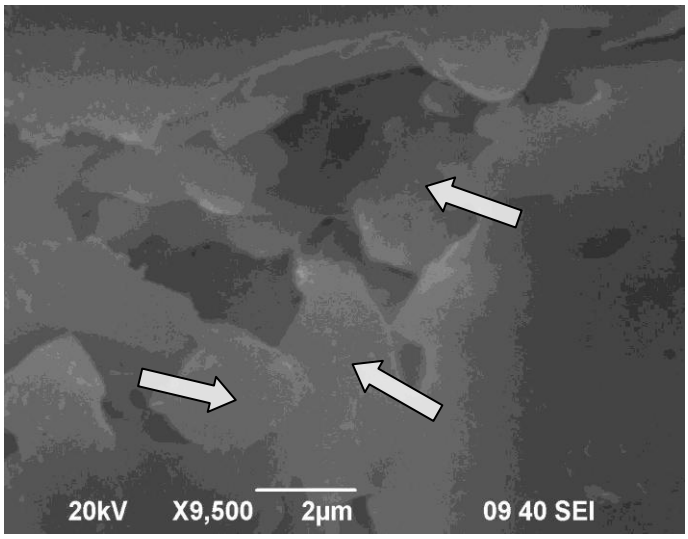

c)

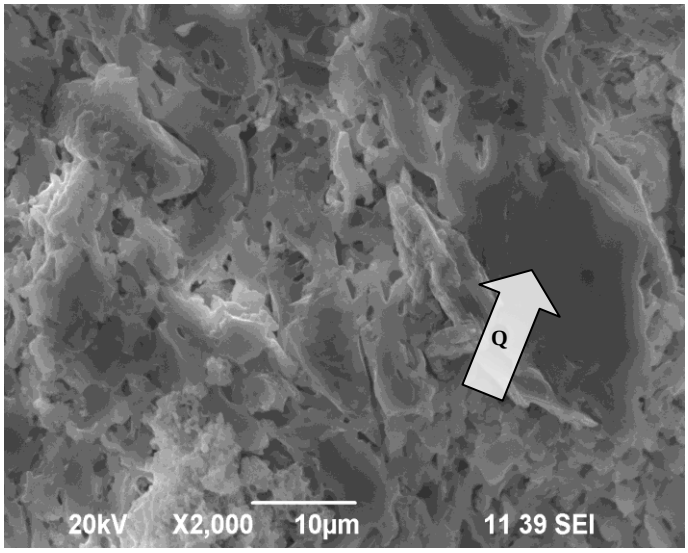

d)

Fig. 10.

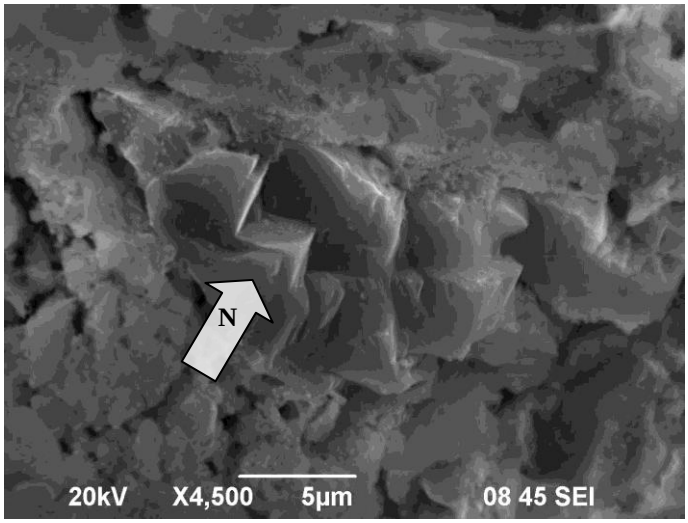

a)

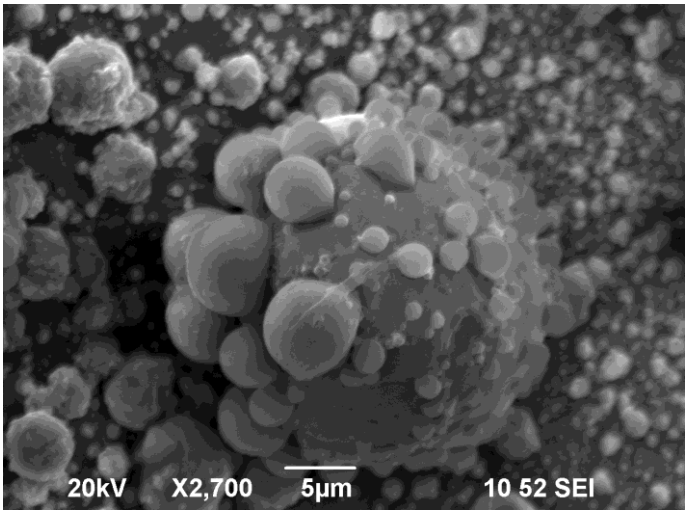

b)

Fig.11.